Solid Earth Discuss., doi:10.5194/se-2016-40, 2016
Manuscript under review for journal Solid Earth
Published: 21 March 2016

Solid Earth Discussions
Open Access
EGU

4D imaging of sub-second dynamics in pore-scale processes using real time synchrotron x-ray tomography

Katherine J. Dobson[1], Sophia B. Coban[2], Sam A. McDonald[3], Joanna Walsh[3], Robert Atwood[4], Philip J. Withers[3]

[1] Ludwig-Maximilians-Universität München, Department für Geo-und Umweltwissenschaften, 80333, Germany.
[2] School of Mathematics, University of Manchester, School of Materials, Manchester, M13 9PL, UK.
[3] School of Materials, University of Manchester, School of Materials, Manchester, M13 9PL, UK.
[4] Diamond Light Source, Harwell Innovation Campus, Didcot, OX11 0DE, UK.

Correspondence to: Katherine J. Dobson (kate.dobson@min.uni-muenchen.de)

Abstract. A variable volume flow cell has been integrated with state-of-the-art ultra-high speed synchrotron x-ray tomography imaging. The combination allows the first real time (sub-second) capture of dynamic pore (micron) scale fluid transport processes in 4D (3D + time). With 3D data volumes acquired at up to 20 Hz, we perform in situ experiments that capture high frequency pore-scale dynamics in 5-25 mm diameter samples with voxel (3D equivalent of a pixel) resolution of 2.5 to 3.8 µm. The data are free from motion artefacts, can be spatially registered or collected in the same orientation making them suitable for detailed quantitative analysis of the dynamic fluid distribution pathways and processes. The method presented here are capable of capturing a wide range of high frequency non equilibrium pore-scale processes including wetting, dilution, mixing and reaction phenomena, without sacrificing significant spatial resolution. As well as fast streaming (continuous acquisition) at 20 Hz, it also allows larger-scale and longer term experimental runs to be sampled intermittently at lower frequency (time-lapse imaging); benefiting from fast image acquisition rates to prevent motion blur in highly dynamic systems. This marks a major technical breakthrough for quantification of high frequency pore scale processes: processes that are critical for developing and validating more accurate multiscale flow models through spatially and temporally heterogeneous pore networks.

Keywords: x-ray tomography, synchrotron, ultra high speed imaging, dynamic tomography, 4D tomography, multi-phase flow

Solid Earth Discuss., doi:10.5194/se-2016-40, 2016
Manuscript under review for journal Solid Earth
Published: 21 March 2016

1 Introduction

Porosity, permeability and flow in geological systems are all highly dynamic. Changes in the confining conditions (e.g. pressure, temperature), flow volume, fluid chemistry/viscosity or suspension composition can drive mass transport (through processes such as precipitation, dissolution, deposition or erosion) and change the connectivity and tortuosity of the pore network. The evolving porosity and permeability then cause further changes in both micro and macro-scale flow. These mass transport processes and the passage of fluid-fluid and fluid-rock reaction fronts through heterogeneous geological system occur at the pore scale. Developing detailed understanding of macroscopic processes as diverse as pollutant transport, hydrocarbon recovery, CO_2 sequestration, storage of nuclear waste, aquifer management, nutrient bio-accessibility, building stone preservation and hydrothermal deposit formation require understanding of multi-scale effect of pore-scale processes.

1.1. Synchrotron imaging for dynamic geoscience applications

Laboratory and synchrotron X-ray computed micro tomography (usually XCT & sXCT respectively) are ideal approaches for imaging these processes as they allow in situ observation in a high resolution non-destructive way. The general principles of X-ray tomography, reconstruction and data processing as relating to geoscience applications are covered in a series of recent reviews (Bultreys et al., 2016; Cnudde and Boone, 2013; Hess et al., 2011; Maire and Withers, 2014; Wildenschild and Sheppard, 2013). For the specific application of understanding pore scale processes, XCT and sXCT are now becoming widely used for both qualitative and quantitative imaging of the complex natural pore networks, and the distribution of liquid(s) within them (Al-Raoush et al., 2011; Al-Raoush and Willson, 2005; Berg et al., 2013; Bhreasail et al., 2012; Boone et al., 2014; Bultreys et al.; Cnudde and Boone, 2013; Dewanckele et al., 2012; Geraud et al., 2003; Herring et al., 2013; Iglauer et al., 2011; Katuwal et al., 2015; Ma et al., 2016; Naveed et al., 2013b; Olafuyi et al., 2010; Sakellariou et al., 2003; Sok et al., 2010; Wildenschild et al., 2002; Wildenschild and Sheppard, 2013) The data are also being used to inform numerical simulations (Al-Raoush and Papadopoulos, 2010; Alhashmi et al., 2015; Bultreys et al., 2016; Bultreys et al., 2015; Degruyter et al., 2010; Menke et al., 2015; Naveed et al., 2013a; Raeini et al., 2015; Raeini et al., 2014; Walter Fourie et al., 2007).

Standard operation is to collect a set of 2D “projections” or “radiographs” at constant angular density while the sample is rotated through 180° or 360°. Standard 3D tomographic images require seconds (synchrotron), minutes (synchrotron and laboratory) or even hours (laboratory) to acquire (Maire and Withers, 2014). Until recently this has limited 3D experimental investigations of dynamic processes because the critical pore scale processes occur over much shorter durations. Many key fluid-rock and fluid-fluid interactions therefore remain poorly constrained. Furthermore, while numerical simulations can now consider multiple mass and thermal transport processes simultaneously and can incorporate realistic pore geometries (see

Solid Earth Discuss., doi:10.5194/se-2016-40, 2016
Manuscript under review for journal Solid Earth
Published: 21 March 2016

Bultreys et al., 2016 for in depth review), many generally still lack validation from experimental data from natural systems where observations are needed with a range of temporal and spatial resolutions.

In recent years, careful alignment of 3D datasets collected at fixed time points over moderate duration experiments has enabled "time integrated" tomography as a tool for quantification of fluid dynamics and porosity evolution (Andrew et al., 2014; Andrew et al., 2015; Armstrong et al., 2014a; Berg et al., 2013; Blunt et al., 2013; Herring et al., 2014; Herring et al., 2013; Lin et al., 2016; Menke et al., 2015; Wildenschild and Sheppard, 2013). The increased image acquisition rates now available at 3rd generation synchrotron facilities has driven development of faster "continuous" imaging. In this mode, samples rotation is not stopped for each projection, instead data is acquired over a narrow arc (typically 0.1-0.5°). For most geological materials collection of the projection data can be just a few seconds (Andrew et al., 2015; Berg et al., 2013; Bhreasail et al., 2012; Pistone et al., 2015; Pistone et al., 2013; Youssef et al., 2014). However, 2D imaging (the same projection acquisition rates but without rotation) is still needed to observe processes occurring on the millisecond-few second timescales; such as individual Haynes jumps and the subsequent relaxation dynamics (Armstrong et al., 2014b; Berg et al., 2013). 2D imaging cannot capture pore, and pore-fluid interface morphology, pore throat orientation and size, or the location of the events within the fluid volume.

Advances in temporal resolution through camera and beam line technology have been followed by highly parallelised iterative reconstruction methods which can use far fewer projections yet still achieve adequate reconstructed image quality (Batenburg and Sijbers, 2011; Brabant et al., 2014; Kaestner et al., 2015; Kazantsev et al., 2015a; Kazantsev et al., 2015b; Van Eyndhoven et al., 2015). However, direct in situ observation of sub-second events and processes, and those that cause rapid change over longer durations still remains challenging. Pushing time integrated tomography towards true long duration 4D imaging would therefore have high impact on our understanding of pore scale processes.

Here we present a state-of-the-art 4D (3D + real time) imaging methodology that enables visualization and quantitative assessment of dynamic pore scale processes in real time (3D acquisition rates of up to 20 Hz) over variable experimental durations. We present two key methodology developments: sub-second real time imaging of fluid transport up to an odder of magnitude faster than previously presented, and the extension of that imaging protocol to allow slower or variable flow dynamics to be quantitatively assessed over longer time periods. We illustrate these potential of the developments for providing insight into pore-scale processes using three case studies showing preliminary data from experiments that quantify initial wetting, the evolution from dynamic to steady state flow, and the evolution of the reaction front during chemical dilution or fluid mixing.

Solid Earth Discuss., doi:10.5194/se-2016-40, 2016
Manuscript under review for journal Solid Earth
Published: 21 March 2016

2 Experimental set up

Disaggregated sandstone gravels (1-2, or 2-4 mm size fraction) were loaded into reusable cylindrical gravity fed flow cell and mounted on the JEEP i12 beamline (Diamond Light Source, Harwell, UK) (Figure 1). Full beam specification can be found in Drakopoulos et al. (2015). The cell diameter for this system can be varied (up to 50 mm diameter) according to experimental need and x-ray transmission through the sample. Perspex sample chambers of 6 and 25 mm internal diameter cells used here. A circular piece of fine mesh was placed at the bottom of the cell above the outlet feed prevented fine material being washed through to the outflow reservoir (maximum volume 125 ml in the configuration used). Particles were added to a minimum depth of 15 mm to ensure no effects from basal flow were observed in the imaging field of view. Particle diameters were sufficiently small that the influence of the cell geometry on particle packing was minimal. The random nature of the packing structure was checked before each experiment during the collection of a single tomography data set (Figure 2).

In the configuration used here, fluid was supplied at a constant flow rate by a 12 channel peristaltic pump operated from the beam line control room (outside the x-ray enclosure or "hutch") so that flow rates and compositions could be adjusted in real time. i.e., while 3D data are being acquired. The inlet tube was attached centrally to the top of the cell using a slip ring to ensure a fixed drip point (approx. 5 mm above the centre of the rotating sample). Flow rates were varied from 40-200 µl/min, which corresponded to a drip every 2 and 10 seconds. The majority of experimental runs were performed using a 6 M KI solution to ensure high contrast between air, fluid and rock particles. Pilot scans showed un-doped H_2O and some oils could be observed under the hard x-rays of the JEEP white beam (50-150 kV), although low contrast would make post-processing challenging.

The flow cell was designed to be easily modified; and can accommodate base fed laminar flows, simultaneous flow of multiple fluids (variable composition or temperature), or multi-phase suspensions. Thin walled (1 mm) aluminium sample chambers can be used for both thermal and pressure variable experiments. The cell can be loaded with disaggregated material (e.g. soil, sand, gravel, glass beads) or with more coherent cored soil/rock samples of any diameter. However, when designing ultra high speed experiments or processes that cause subtle changes in attenuation/composition, higher density or large volume solid samples will increase the minimum exposure time and may also cause artefacts that reduce the ability to resolve features of interest.

3 Ultra-fast image acquisition

The maximum rotation speed of the JEEP tomography stage is 10 Hz (continuous rotation). As synchrotron tomography datasets are acquired over 180°, 3D volumes can be acquired at up to 20 Hz. The actual operational rotation speed for given experiment will be controlled by the exposure time for each projection and the total number of projections collected per 3D

Solid Earth Discuss., doi:10.5194/se-2016-40, 2016
Manuscript under review for journal Solid Earth
Published: 21 March 2016

data set. Exposure time is controlled by x-ray flux and sample density. Imaging at the JEEP beam line can be performed using a polychromatic (white) or monochromatic x-ray beam (selectable energy range 53-150 kV). Images were acquired using a Vision Research Phantom Miro™ 310M camera (up to 5000 frames per second). In white beam mode exposure times for the large diameter cell were 200 µs (3.8 µm pixel resolution), dropping to 90 µs for the smaller diameter system (2.5 µm pixel resolution). The diameter of the samples used here exceeds the field of view of the highest magnification module available at JEEP (1.25 µm pixel resolution), but region of interest images could be obtained with a 200 µs exposure.

In most "traditional" tomography experiments, over 1000 projections are collected for each 3D volume. We collected high resolution data (1800 projections, 0.2 and 0.5 s per 3D data acquisition) for each dry sample prior to flow initiation to characterise the inter- and intra-grain porosity of each sample (Figure 2A, B). This data can also be used as a structural prior for iterative reconstruction methods (e.g.; Kazantsev et al. 2015 a, b; van Eyndhoven et al 2015). Reducing the angular density of the projections will shorten overall scan time. The reconstructed image quality does reduce as the projection density drops, but a significant increase in temporal resolution can be achieved. To achieve the maximum 20 Hz 3D image acquisition rate, it is necessary to reduce the number of projections to 250 (200 µs exposure) and 550 (90 µs exposure) per scan.

Under-sampling (using fewer projections) to this degree does cause image quality to degrade, making differences between phases of similar attenuation hard to observe, and reducing the precision with which phase boundaries and volumes can be defined. When features of interest are relatively small, or have complex geometries then under-sampling can prevent quantitative analysis. However, here the contrast between the saline solution, rock and air is high, and the primary target is the sub-second distribution of the fluid phase. Using the routine filter back projection reconstruction algorithms, testing with as few as 360 (Figure 2C) and 180 projections (Figure 2D) gave adequate images for basic quantification (Figure 2E). Comparison of the two under-sampled data sets shows little increase in quality and little overall change between the 360 and 180 projection scans. For the smaller cells, it is possible to collect 360 projections at maximum image acquisition frequency.

The Miro camera has fixed on board data storage, which for the field of view needed in this experiment allowed a maximum of approximately 20000 projections to be collected (in this set up, the number of projections is dependant on the field of view needed). The under-sampling allowed between 53 and 141 3D data sets to be acquired in a single experimental run (2.5-7 seconds of acquisition at maximum frequency). Capturing a specific event with this short a duration of collection is challenging, especially as the high rotation speeds prevents observation of small volume changes in the live view radiographs. During collection the camera is armed and then triggered. Arming the camera starts projection acquisition, but that data is automatically overwritten until the trigger signal is received. The user can define the trigger to mark a) the last image; all existing projections on the card are saved, b) the first image; projections are collected until the card volume is full, or c) an event; with a user defined number of projections before and after the trigger are saved. The latter option allows a small amount of buffer time for the user to capture a specific event, such as a drip entering the sample, or a flow volume/composition change.

Solid Earth Discuss., doi:10.5194/se-2016-40, 2016
Manuscript under review for journal Solid Earth
Published: 21 March 2016

Automatic triggering mechanisms such as light gates can be incorporated although in this experiment a webcam was used to observe the delivery of each drip.

To clarify the real-time nature of the data, the following terminology is used in all subsequent discussion: one or more scans are collected during each experiment, each scan contains a number of 3D "frames" which were acquired at a known speed, and with a given frequency (defined by the time between the first projections of sequential frames). Data are offloaded from the camera between scans (download takes between 5 and 7 minutes). Several scans can be collected during an experiment. To highlight specific processes and features, most figures presented below show only 2D slices (either perpendicular or parallel to flow) or a sub-volume of the reconstructed data set. The post processing and image segmentation are the same for all examples, and were performed in Avizo™ and MATLAB. The methods are outlined in Appendix 1.

3.1 Case study: Observing sub-second dynamics using ultra-fast imaging

Wetting processes and the formation of rivulet networks are poorly understood in heterogeneous media. The processes operate on short times scales and are strongly influenced by sample morphology. Non-invasive 4D tomography is ideal for capturing the dynamics of these behaviours. Figure 3 shows the evolution of the fluid distribution in a sub volume of the sample immediately below the drip point. The data were collected under continuous acquisition mode, with a frame acquisition frequency of 0.07s (system operating at 7Hz rotation speed).

The first drip of KI solution (shown in blue) enters the dry sandstone bed (rendered in translucent grey) between Frame 0 and Frame 1 (Figure 3). Initially (t = 0.07s) fills the inter-grain pore space to the front of the sub volume (A), and immediately begins lateral transport into the intra-grain porosity in the neighbouring grains (B, Figure 3). By the second frame (t = 0.14s) the inter-grain volume has largely emptied, and the majority of the fluid is now within the grains. Intra-grain transport has also occurred with capillary driven wetting of grains not in direct contact with inter-grain fluid (e.g. C), and from other viewing angles drainage of previously saturated intra-grain pores can also be observed. Between F1 and F2 most grains in contact with the inter-grain fluid have become partially or fully saturated. The remaining intra-grain fluid is generally limited to a few small pores, and surface films (D). The figure only shows the relaxation after the first drip. As the experiment continues (F3 to F5), the fluid is moves away from the initial location, with grain saturation increasing by radial and vertical redistribution, with upward propagation of the saturation front in some instances (E). Most grains show and expansion and coalescence of grain-surface fluid films after initial intra-grain saturation (F), although grain surface wetting does occur with no, or prior to intra-grain saturation (G). Capillary forces continue to redistribute the intra-grain pore fluid over the remainder of the experiment, with saturation of many grains decreasing as the system moves towards equilibrium. Grains at both the upper and lower extent of the wetted region (H) are almost completely saturated and then drained again within 1.54 seconds.

Solid Earth Discuss., doi:10.5194/se-2016-40, 2016
Manuscript under review for journal Solid Earth
Published: 21 March 2016

Vertical slices taken through the same sub-volume of the sample in the second scan of the experiment shows the arrival of the third drip (Figure 4). In this experiment the fluid feed was stopped during data download. When the pump was restarted, the first drip was used as the trigger the scan acquisition. The initial frames of the second scan were before the arrival of the drip, and act as a wet reference. Differences in the fluid volume across the download period result from the fall of a drip at the very end of the experiment, immediately after fluid feed was stopped. Figure 4 captures the major changes in the fluid distribution in the inter-grain porosity (blue). At this time, the intra-grain fluid distribution (grey) has become largely stable, although a few grains still show some variability (B, Figure 4).

Passage of the drip causes transient fluid bridging (A; Figure 4). Most bridging connections are maintained throughout the drip cycle, but some transient connections are formed with every drip, and others form only occasionally. Temporary isolation of fluid (enhanced by capillary driven draw in of the surface film during equilibration as observed at A; Figure 4) could control chemical reaction rates in reactive systems. Upon reconnection the relatively small volume of this fluid would be rapidly diluted, but rates of dissolution etc. would be locally reduced by limited fluid supply. A later part of the experiment is shown in Movie 1 (see Supplementary Material).

Although the focus of this contribution is on method development, we include a limited selection of the quantitative analysis performed on these samples, as an illustration of the adequacy of the data quality. Quantitative analysis of inter- and intra-grain fluid volume shows the strong fluctuation over the course of two drips (Figure 5) and the general instability of the fluid volume as it is redistributed. After the first drip, the saturation of the intra-grain porosity becomes more gradual, with significant increases on the arrival of subsequent drips. The inter-grain distribution equilibrates more slowly.

4 Ultra-high speed imaging for longer experimental durations

The short duration experiments presented above allow capture of the high speed dynamics, but have very short overall durations (< 10 seconds). Capturing longer duration processes with the same 3D frame acquisition rates requires lower frame acquisition frequencies. The Miro camera allows data to be acquired either continuously (as above) or over the same 180° arc with a user defined rotation angle between acquisitions (hereafter gapped acquisition). Gapped acquisition decreases frame acquisition frequency, while maintaining frame acquisition speeds, and the resultant data therefore benefits from a lack of motion induced blurring in the reconstructed data.

Although any angular gap can be defined, gaps were limited to multiples of 180° for simplicity. This ensures that the initial projection of every frame was collected at the either 0° or 180° with respect to the first projection in the scan. Registration of the data in this manner saves significant time in post processing. A gapped acquisition with a spacing of 1 (G1) collects over

Solid Earth Discuss., doi:10.5194/se-2016-40, 2016
Manuscript under review for journal Solid Earth
Published: 21 March 2016

the 0-180° sector of every rotation (1 full rotation between acquisition start points); a gapped acquisition with spacing of 5 (G5) acquires from 0-180° on every third rotation (3 full rotations between acquisition start points).

Although not used in this experiment, the camera memory can also be partitioned allowing for a fixed number of projections/frames in each partition. This would enable a imaging across different temporal scales in one scan.

4.1 Case study: Capturing multi-scale dynamics in pore-scale processes

To show the suitability of this method for capturing the variability of pore-scale flow dynamics, wetting experiments were scanned repeatedly at different gap lengths (continuous through to G25). Between 53 and 106 frames were collected in each scan. High frequency data acquisition (continuous or G1) was used to capture the first few drips, with longer acquisition intervals (G3-G25) used to capture the slower processes as the flow network evolved towards steady state through time (Figure 6). In some experimental runs, variability in the high speed processes through time was also assessed, by repeating continuous, G1 or G3 acquisition at intervals between G5 or G7 acquisitions.

The larger fluid volume in these images for longer durations experiments makes visualisation of the 3D fluid distribution challenging to show on the page (as in Figure 3), and so a semi-transparent render of a distance map is used to show the variability in the local fluid volume (Figure 6). Areas of inter-grain fluid appear as red regions, while the majority of the intra-grain fluid is shown in blue and green. In all scans at all frame acquisition frequencies, we see significant variability in the distribution of the KI solution (Figure 6) over the 35-60 minute experiments.

From the same data it is possible track the local changes in saturation on the grain-scale. Well established network analysis and morphological quantification algorithms can be applied to extract details of saturation on the pore scale (Figure 7) or on the geometry of individual phase interfaces and contact angles (Andrew et al. 2014, 2015). For under-sampled data higher levels of image noise in filtered back projection reconstructions may limit quantitative surface curvature and contact angle analysis, but optimised iterative reconstruction methods may give more suitable data (see Section 5 below).

4.2 Case Study: In situ observation of mixing dynamics

One key application for ultra-high speed in situ imaging is to track the interaction between multiple phases: capturing both spatial and temporal heterogeneity of replacement, dilution and chemical reactions. After 30 mins under a 6M saline feed the system was flushed with H2O. Scanning was performed at G1 (0.07 s scan acquisition time, 7 Hz acquisition frequency), the scan started on arrival of the first H2O drip. Other experimental runs tested replacing H2O with KI solution, and replacing oil with KI solution. The need for ultra-high speed imaging to capture the complex and spatially variable mixing and dilution processes can be seen in Figure 9. Dilution of the uppermost part of the local inter-grain network is instantaneous (Figure 9

Solid Earth Discuss., doi:10.5194/se-2016-40, 2016
Manuscript under review for journal Solid Earth
Published: 21 March 2016

A), but percolation of the dilution/replacement front through the image volume takes approximately 5 seconds (Figure 9 A-F). After this time there is little major change in the local greyscale values (Figure 9 G,H) implying a shift in mixing mechanisms. The 2D slices through the same sub volume perpendicular to the flow direction (Figure 9) show the dilution is extremely heterogeneous and can occur on a range of timescales in neighbouring regions. The central pore volume (orange box, F30) is diluted over 10-15 scans, whereas a neighbouring region (connected in 3D) is replaced in under 5 frames (yellow box F35). Some grains show variability in the KI concentration within the porosity, implying that although the bulk porosity of this sandstone is approx. 20%, and the connectivity is high, individual grains have discrete pore networks within them (blue boxes F45). Using slower data acquisition methods would not capture the dynamics of replacement.

5 Moving beyond the state-of-the art

The ultra-high imaging presented here allows capture of wetting and transport behaviour at the moderate-to-high spatial resolution necessary for quantitative understanding of the processes involved. The 3D frame acquisition speed and frequency are substantially faster that has been previously achieved. Events such as Hayne jumps (millisecond time-scale), and the subsequent relaxation (a few seconds) have been observed in 2D imaging (acquisition of projections without rotation) (Armstrong et al., 2014b). The method presented here can provide data on the 3D nature of those changes, at comparable timescales. Such quantitative data can be used to develop or validate larger scale flow models and to better incorporate pore scale processes.

The data presented here are reconstructed using standard filtered back projection reconstruction algorithms. However, these methods are not optimal for under sampled data. Recent advances in iterative reconstruction algorithms use information about the different phases contained within the data, to enhance the quality of the reconstruction, with great effect (Figure 9). Visual comparison of this type of method (Figure 9 B, D) with reconstructions using filtered back projection (Figure 9 A, C) shows the improvement in phase resolution that can be achieved on fewer projection data. This example applies an iterative optimisation solver, and along total variation penalisation is incorporated as a regularisation step (Rudin et.al.,1992; Little and Jones, 2010) that takes the sample porosity into account (i.e. uses the data itself as prior information), with refinement at each iteration. The iterative data have fewer line artefacts and lower noise, and permits accurate phase segmentation from fewer than 45 projections.

Iterative methods have significant potential to develop imaging dynamic pore-scale processes still further. Of specific interest are those methods that use high quality dry scan data as a structural prior (Kazantsev et al., 2014; Kazantsev et al., 2015a; Kazantsev et al., 2015c; Van Eyndhoven et al., 2015), and those that divide the data volume into static and dynamic regions using the static information from sequential scans to better define the reconstruction volume Kazantsev et al., 2014; Kazantsev et al., 2015a; Kazantsev et al., 2015c; Van Eyndhoven et al., 2015). Both allow reconstruction of better quality images from

Solid Earth Discuss., doi:10.5194/se-2016-40, 2016
Manuscript under review for journal Solid Earth
Published: 21 March 2016

under-sampled data (data with fewer projections) and also allow data of comparable or better quality to that displayed here to be produced from data sets with as few as 18 projections (Van Eyndhoven et al., 2015). These methods can improve the quality of the quantitative data, especially on the key phase interfaces, however the key advance is likely to come from working with still higher degrees of under-sampling.

At the 3D volume acquisition rates achieved here, the projection exposure times and mechanical limit of the rotation stage means that imaging faster is not currently possible for the current samples. For higher density materials, or higher resolution cameras where longer exposure times mean slower overall volume acquisition, iterative methods may improve temporal resolution. However, on the JEEP experimental set up, the main advantage of iterative methods is the ability to acquire fewer projections per scan and so collect more scans per experiment without sacrificing image quality. This could enable experimental run times to be extended by up to an order of magnitude.

The methods presented here provide a workflow for visualization and quantification of sub-second dynamics in porous media (Figure 10). The method is not limited to the simple drip-fed experiments presented here, and can be easily applied to high speed processes operating in geological materials at temperature or undergoing deformation. The ability of the experimental set up to acquire large numbers of projections at constant angular density means that even higher temporal resolution could be achieved. Reconstruction of volumes from data sets with small rotational offsets (typically about 10-20 degrees, i.e. Scan 1 reconstruction from 0-180°, Scan 2 reconstruction from 10-190° etc.) could increase temporal resolution by over an order of magnitude (Van Eyndhoven et al. 2015), especially when coupled to iterative methods that can reduce image noise, and enhance phase boundary definition in the reconstructed data.

Complex multi-phase, spatially heterogeneous micro- and pore-scale processes control so many macro-scale geological system responses. The development of ultra-high speed imaging mean that quantitative understanding of these processes is now possible.

Solid Earth Discuss., doi:10.5194/se-2016-40, 2016
Manuscript under review for journal Solid Earth
Published: 21 March 2016

6 Appendix 1

6.1 Post processing and image analysis

Visualisation and quantification was performed using Avizo™ and MATLAB. The greyscale volumes were cropped to the sample boundaries to reduce all subsequent processing times. When processing continuous acquisition data the frames were first aligned to allow direct comparison and quantitative analysis. For the gapped scans, all data are acquired over the same angle and no additional alignment is required. The italicised steps in the following refer to built in algorithms in Avizo™, and the reader is directed to the associated documentation for further details of the implementation.

An edge preserving *Bilateral Filter* was applied to the greyscale filtered back projection reconstructions to reduce image noise. Water, air and rock phases were segmented using the *Interactive Thresholding*, and the resultant binary data volumes were used in subsequent analysis. The inter- and intra-grain porosity was defined by creating two separate binary masks: one by segmentation of the wet and dry grains, and one by segmentation of the fluid (inter-and intra-granular). Logical combination of these allows calculation of the inter- and intra-granular fluid volumes. Fluid volumes were calculated using in-built image measures, (*Volume3D).*

Additional quantitative analysis of the intra-grain porosity was performed on single grains isolated using the MATLAB command imfill followed by *Watershed segmentation*. The pore network within the grain was displayed using the *Centerline Tree* module which applies the TEASAR algorithm (Sato et al. 2000) defining local Euclidian distance to the nearest object boundary. Fluid thickness was calculated by applying a Chamfer 3D distance map to the fluid label volume to calculate the distance to the nearest surface. The exchange of KI for H_2O was tracked by calculating a differential image between the initial scan and each subsequent frame.

Solid Earth Discuss., doi:10.5194/se-2016-40, 2016
Manuscript under review for journal Solid Earth
Published: 21 March 2016

7 Author contribution

The study was designed by KJD and SAM, reconstruction and visualisation was led by SBC & KJD with assistance from SAB. RA led camera integration at Diamond Light Source. KJD, SBC, SAM, JW & RA performed the experiments at i12/JEEP. The lead author was KJD, with all other authors contributing to the manuscript.

8 Acknowledgements

KJD is supported by EVOKES ERC247076 and NERC NE/M018678/1, SBC is supported by EPSRC EP/J010456/1, the School of Mathematics, and the BP International Centre for Advanced Materials. PJW wishes to acknowledge the BP International Centre for Advanced Materials for funding under ICAM 03. SAM is grateful to Zeiss for funding his fellowship. We thank Diamond Light Source for access to beamline I12 (beam time award EE10500-1).

Solid Earth Discuss., doi:10.5194/se-2016-40, 2016
Manuscript under review for journal Solid Earth
Published: 21 March 2016

9 References

Al-Raoush, R., Gordon, C., Robins, S., Richardson, J., 2011. Characterization of immiscible non-wetting fluids in porous media systems using synchrotron tomography. Abstracts of Papers of the American Chemical Society 241, 1.

Al-Raoush, R., Papadopoulos, A., 2010. Representative elementary volume analysis of porous media using X-ray computed tomography. Powder Technology 200, 69-77.

Al-Raoush, R.I., Willson, C.S., 2005. Extraction of physically realistic pore network properties from three-dimensional synchrotron X-ray microtomography images of unconsolidated porous media systems. Journal of Hydrology 300, 44-64.

Alhashmi, Z., Blunt, M.J., Bijeljic, B., 2015. Predictions of dynamic changes in reaction rates as a consequence of incomplete mixing using pore scale reactive transport modeling on images of porous media. Journal of Contaminant Hydrology 179, 171-181.

Andrew, M., Bijeljic, B., Blunt, M.J., 2014. Pore-by-pore capillary pressure measurements using X-ray microtomography at reservoir conditions: Curvature, snap-off, and remobilization of residual CO2. Water Resources Research 50, 8760-8774.

Andrew, M., Menke, H., Blunt, M.J., Bijeljic, B., 2015. The Imaging of Dynamic Multiphase Fluid Flow Using Synchrotron-Based X-ray Microtomography at Reservoir Conditions. Transp Porous Med 110, 1-24.

Armstrong, R.T., Georgiadis, A., Ott, H., Klemin, D., Berg, S., 2014a. Critical capillary number: desaturation studied with fast X-ray computed microtomography. Geophys. Res. Lett. 41, 55-60

Armstrong, R.T., Ott, H., Georgiadis, A., Rucker, M., Schwing, A., Berg, S., 2014b. Subsecond pore-scale displacement processes and relaxation dynamics in multiphase flow. Water Resources Research 50, 9162-9176.

Batenburg, K.J., Sijbers, J., 2011. DART: A Practical Reconstruction Algorithm for Discrete Tomography. IEEE Transactions on Image Processing 20, 2542-2553.

Berg, S., Ott, H., Klapp, S.A., Schwing, A., Neiteler, R., Brussee, N., Makurat, A., Leu, L., Enzmann, F., Schwarz, J.-O., Kersten, M., Irvine, S., Stampanoni, M., 2013. Real-time 3D imaging of Haines jumps in porous media flow. . Proceedings of the National Academy of Sciences 110 3755-3759.

Bhreasail, Á.N., Lee, P.D., O'Sullivan, C., Fenton, C.H., Hamilton, R., Rockett, P., Connolley, T., 2012. In-Situ Observation of Cracks in Frozen Soil using Synchrotron Tomography. Permafrost and Periglacial Processes 23, 170-176.

Blunt, M.J., Bijeljic, B., Dong, H., Gharbi, O., Iglauer, S., Mostaghimi, P., Paluszny, A., Pentland, C., 2013. Pore-scale imaging and modelling. Advances in Water Resources 51, 197-216.

Boone, M.A., De Kock, T., Bultreys, T., De Schutter, G., Vontobel, P., Van Hoorebeke, L., Cnudde, V., 2014. 3D mapping of water in oolithic limestone at atmospheric and vacuum saturation using X-ray micro-CT differential imaging. Materials Characterization 97, 150-160.

Brabant, L., Dierick, M., Pauwels, E., Boone, M.N., Van Hoorebeke, L., 2014. EDART, a discrete algebraic reconstructing technique for experimental data obtained with high resolution computed tomography. Journal of X-Ray Science and Technology 22, 47-61.

Bultreys, T., Boone, M.A., Boone, M.N., De Schryver, T., Masschaele, B., Van Hoorebeke, L., Cnudde, V., (2016) Fast laboratory-based micro-computed tomography for pore-scale research: Illustrative experiments and perspectives on the future. Advances in Water Resources.

Bultreys, T., De Boever, W., Cnudde, V., 2016. Imaging and image-based fluid transport modeling at the pore scale in geological materials: A practical introduction to the current state-of-the-art. Earth-Science Reviews 155, 93-128.

Bultreys, T., Van Hoorebeke, L., Cnudde, V., 2015. Multi-scale, micro-computed tomography-based pore network models to simulate drainage in heterogeneous rocks. Advances in Water Resources 78, 36-49.

Cnudde, V., Boone, M.N., 2013. High-resolution X-ray computed tomography in geosciences: A review of the current technology and applications. Earth-Science Reviews 123, 1-17.

Degruyter, W., Burgisser, A., Bachmann, O., Malaspinas, O., 2010. Synchrotron X-ray microtomography and lattice Boltzmann simulations of gas flow through volcanic pumices. Geosphere 6, 470-481.

Dewanckele, J., De Kock, T., Boone, M.A., Cnudde, V., Brabant, L., Boone, M.N., Fronteau, G., Van Hoorebeke, L., Jacobs, P., 2012. 4D imaging and quantification of pore structure modifications inside natural building stones by means of high resolution X-ray CT. Science of The Total Environment 416, 436-448.

Drakopoulos, M., Connolley, T., Reinhard, C., Atwood, R., Magdysyuk, O., Vo, N., Hart, M., Connor, L., Humphreys, B., Howell, G., Davies, S., Hill, T., Wilkin, G., Pedersen, U., Foster, A., De Maio, N., Basham, M., Yuan, F., Wanelik, K., 2015. I12: the Joint Engineering, Environment and Processing (JEEP) beamline at Diamond Light Source. Journal of Synchrotron Radiation 22, 828-838.

Solid Earth Discuss., doi:10.5194/se-2016-40, 2016
Manuscript under review for journal Solid Earth
Published: 21 March 2016

Geraud, Y., Surma, F., Mazerolle, F., 2003. Porosity and fluid flow characterization of granite by capillary wetting using X-ray computed tomography. Geological Society, London, Special Publications 215, 95-105.

Herring, A.L., Andersson, L., Newell, D.L., Carey, J.W., Wildenschild, D., 2014. Pore-scale observations of supercritical CO2 drainage in Bentheimer sandstone by synchrotron x-ray imaging. International Journal of Greenhouse Gas Control 25, 93-101.

Herring, A.L., Harper, E.J., Andersson, L., Sheppard, A., Bay, B.K., Wildenschild, D., 2013. Effect of fluid topology on residual nonwetting phase trapping: Implications for geologic CO2 sequestration. Advances in Water Resources 62, Part A, 47-58.

Hess, K.U., Flaws, A., Muehlbauer, M.J., Schillinger, B., Franz, A., Schulz, M., Calzada, E., Dingwell, D.B., Bente, K., 2011. Advances in high-resolution neutron computed tomography: Adapted to the earth sciences. Geosphere 7, 1294-1302.

Iglauer, S., Paluszny, A., Pentland, C.H., Blunt, M.J., 2011. Residual CO2 imaged with X-ray micro-tomography. Geophysical Research Letters 38, 6.

Kaestner, A., Trtik, P., Zarebandkouki, M., Kazantsev, D., Snehota, M., Dobson, K., Lehmann, E., 2015. Recent developments in neutron imaging with applications for porous media research. Solid Earth Discussions 7.

Katuwal, S., Norgaard, T., Moldrup, P., Lamande, M., Wildenschild, D., de Jonge, L.W., 2015. Linking air and water transport in intact soils to macropore characteristics inferred from X-ray computed tomography. Geoderma 237, 9-20.

Kazantsev, D., S., O., Hutton, B. F., Dobson, K.J., Kaestner, A.P., Lionheart, W.R.B., J., W.P., Lee, P.D., Arridge, S.R., 2014. A novel technique to incorporate structural prior information into multi-modal tomographic reconstruction. Inverse Problems 30, 065004.

Kazantsev, D., Thompson, W.M., Van Eyndhoven, G., Dobson, K., Kaestner, A.P., Lionheart, W., Withers, P.J., Lee, P.D., 2015a. 4D-CT reconstruction with unified spatial-temporal patch-based regularization. Inverse Problems Imaging 9, 447-467.

Kazantsev, D., Van Eyndhoven, G., Lionheart, W., Withers, P., Dobson, K., McDonald, S., Atwood, R., Lee, P., 2015b. Employing temporal self-similarity across the entire time domain in computed tomography reconstruction. Philosophical Transactions of the Royal Society of London A. 373, 20140389.

Kazantsev, D., Van Eyndhoven, G., Lionheart, W.R.B., Withers, P.J., Dobson, K.J., McDonald, S.A., Atwood, R., Lee, P.D., 2015c. Employing temporal self-similarity across the entire time domain in computed tomography reconstruction. Philosophical Transactions of the Royal Society a-Mathematical Physical and Engineering Sciences 373, 14.

Lin, Q., Barker, D.J., Dobson, K.J., Lee, P.D., Neethling, S.J., 2016. Modelling particle scale leach kinetics based on X-ray computed micro-tomography images. Hydrometallurgy 162, 25-36.

Little, M.A., Jones, N.S., 2010. Sparse Bayesian step-filtering for high-throughput analysis of molecular machine dynamics, IEEE International Conference on Acoustics, Speech and Signal Processing, ICASSP 2010 Proceedings Dallas, Texas, USA.4162-4165.

Ma, L., Taylor, K.G., Lee, P.D., Dobson, K.J., Dowey, P.J., Courtois, L., 2016. Novel 3D centimetre-to nano-scale quantification of an organic-rich mudstone: The Carboniferous Bowland Shale, Northern England. Marine and Petroleum Geology 72, 193-205.

Maire, E., Withers, P.J., 2014. Quantitative X-ray tomography. International Materials Reviews 59, 1-43.

Menke, H.P., Bijeljic, B., Andrew, M.G., Blunt, M.J., 2015. Dynamic Three-Dimensional Pore-Scale Imaging of Reaction in a Carbonate at Reservoir Conditions. Environmental Science & Technology 49, 4407-4414.

Naveed, M., Hamamoto, S., Kawamoto, K., Sakaki, T., Takahashi, M., Komatsu, T., Moldrup, P., Lamande, M., Wildenschild, D., Prodanovic, M., de Jonge, L.W., 2013a. Correlating Gas Transport Parameters and X-Ray Computed Tomography Measurements in Porous Media. Soil Science 178, 60-68.

Naveed, M., Moldrup, P., Arthur, E., Wildenschild, D., Eden, M., Lamand, M., Vogel, H.J., de Jonge, L.W., 2013b. Revealing Soil Structure and Functional Macroporosity along a Clay Gradient Using X-ray Computed Tomography. Soil Science Society of America Journal 77, 403-411.

Olafuyi, O.A., Sheppard, A.P., Arns, C.H., Sok, R.M., Cinar, Y., Knackstedt, M.A., Pinczewski, W.V., 2010. Experimental Verification of Effect of Size on Drainage Capillary Pressure Computed from Digitized Tomographic Images. International Journal of Engineering Research in Africa 1, 1-10.

Pistone, M., Arzilli, F., Dobson, K.J., Cordonnier, B., Reusser, E., Ulmer, P., Marone, F., Whittington, A.G., Mancini, L., Fife, J.L., Blundy, J.D., 2015. Gas-driven filter pressing in magmas: Insights into in-situ melt segregation from crystal mushes. Geology 43, 699-702.

Pistone, M., Caricchi, L., Ulmer, P., Reusser, E., Ardia, P., 2013. Rheology of volatile-bearing crystal mushes: Mobilization vs. viscous death. Chemical Geology 345, 16-39.

Raeini, A.Q., Bijeljic, B., Blunt, M.J., 2015. Modelling capillary trapping using finite-volume simulation of two-phase flow directly on micro-CT images. Advances in Water Resources 83, 102-110.

Raeini, A.Q., Blunt, M.J., Bijeljic, B., 2014. Direct simulations of two-phase flow on micro-CT images of porous media and upscaling of pore-scale forces. Advances in Water Resources 74, 116-126.

Rudin,L.I., Osher, S., Fatemi, E., 1992. Nonlinear total variation based noise removal algorithms, Physica D: Nonlinear Phenomena, 60, 1–4, 259-268,

Sakellariou, A., Sawkins, T.J., Senden, T.J., Arns, C.H., Limaye, A., Sheppard, A.P., Sok, R.M., Knackstedt, M.A., Pinczewski, W.V., Berge, L.I., Øren, P.-E., 2003. Micro-CT Facility For Imaging Reservoir Rocks At Pore Scales.

Sato, M.; Bitter, I.; Bender, M.A.; Kaufman, A.E.; Nakajima, M. 2000. TEASAR: tree-structure extraction algorithm for accurate and robust skeletons. , Proceedings of the Eighth Pacific Conference on Computer Graphics and Applications. 281 – 449.

Sok, R.M., Varslot, T., Ghous, A., Latham, S., Sheppard, A.P., Knackstedt, M.A., 2010. Pore Scale Characterization of Carbonates at Multiple Scales: Integration of Micro-CT, BSEM, FIBSEM. PetroPhysics 51, 379.

Van Eyndhoven, G., Batenburg, K.J., Kazantsev, D., Van Nieuwenhove, V., Lee, P.D., Dobson, K.J., Sijbers, J., 2015. An Iterative CT Reconstruction Algorithm for Fast Fluid Flow Imaging. Image Processing, IEEE Transactions on 24, 4446-4458.

Fourie, W., Said, R., Young, P., Barnes, D.L.., 2007. The Simulation of Pore Scale Fluid Flow with Real World Geometries Obtained from X-Ray Computed Tomography, Proceedings of the Boston COMSOL Conference.

Wildenschild, D., Hopmans, J.W., Vaz, C.M.P., Rivers, M.L., Rikard, D., Christensen, B.S.B., 2002. Using X-ray computed tomography in hydrology: systems, resolutions, and limitations. Journal of Hydrology 267, 285-297.

Wildenschild, D., Sheppard, A.P., 2013. X-ray imaging and analysis techniques for quantifying pore-scale structure and processes in subsurface porous medium systems. Advances in Water Resources 51, 217-246.

Youssef, S., Oughanem, R., Rosenberg, E., Maire, E., Mokso, R., 2014. 4D Imaging of Fluid Flow Dynamic in Natural Porous Media by Ultra-fast X-ray Microtomography, International Congress on 3D Materials Science 2014.

Solid Earth Discuss., doi:10.5194/se-2016-40, 2016
Manuscript under review for journal Solid Earth
Published: 21 March 2016

10 Figures

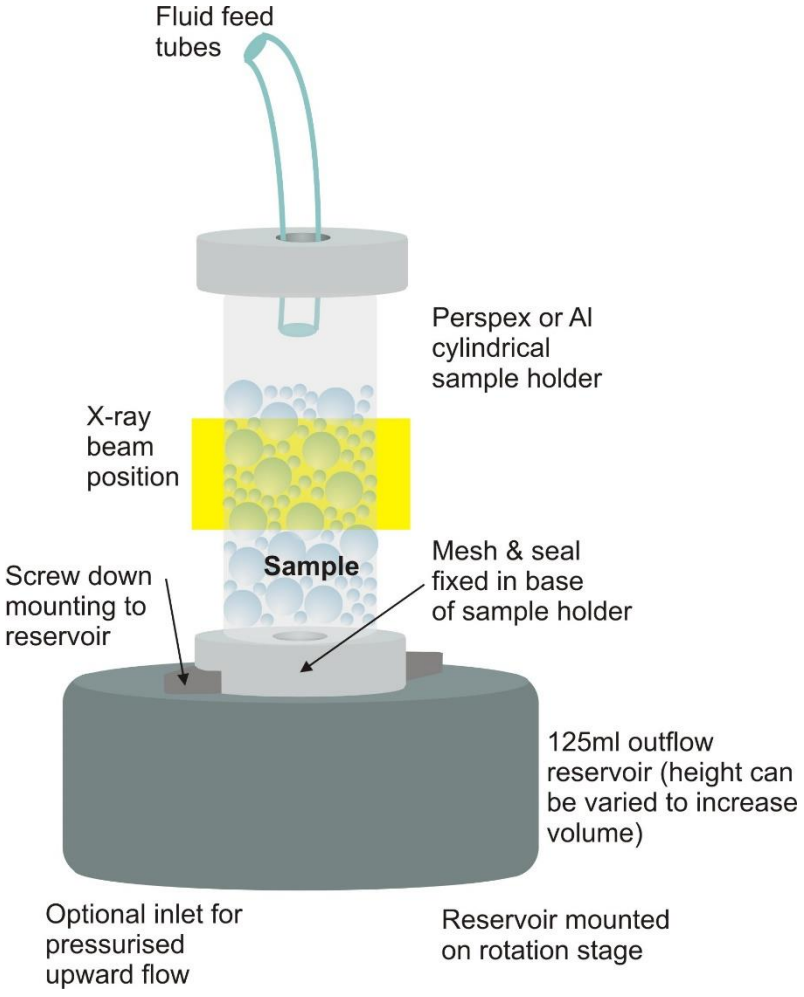

Figure 1: A schematic showing the simple peristaltic pump drip fed gravity driven flow cell. The system was designed to be modifiable to incorporate laminar and multi-phase flow, and to be suitable for use with confining pressure and variable temperatures. All key dimension (sample cell diameter, height & material; reservoir volume; feed) can be adjusted to fit experimental parameters and beam line imaging conditions.

Solid Earth Discuss., doi:10.5194/se-2016-40, 2016
Manuscript under review for journal Solid Earth
Published: 21 March 2016

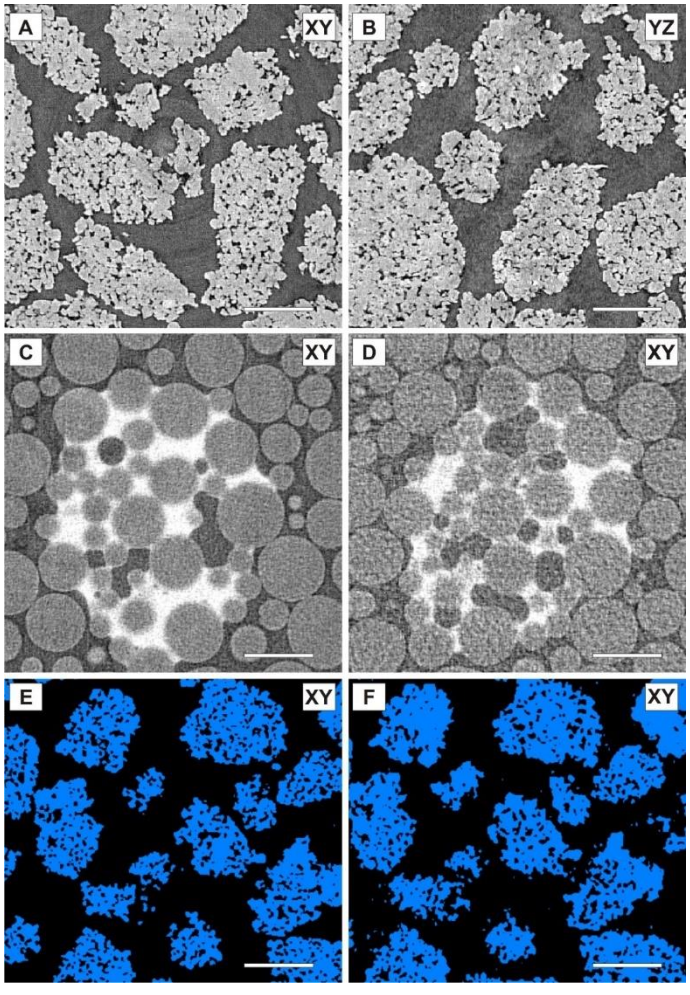

Figure 2: 2D reconstructed slices through a typical gravel sample. High resolution (1800 projection data) perpendicular (A; XY) and parallel to flow direction (B; XZ) reconstructed using filtered back projection. C) A 2D slice (XY) through a simple spherical bad pack containing a small volume for KI solution reconstructed from 360 projections (2/°) using filtered back projection; D) The same 2D slice reconstructed from 180 projections (1/°) using filtered back projection; E & F) Comparison of the segmentation of the rock possible from the 1800 and 180 projection data. All scale bars are 200 µm.

Solid Earth Discuss., doi:10.5194/se-2016-40, 2016
Manuscript under review for journal Solid Earth
Published: 21 March 2016

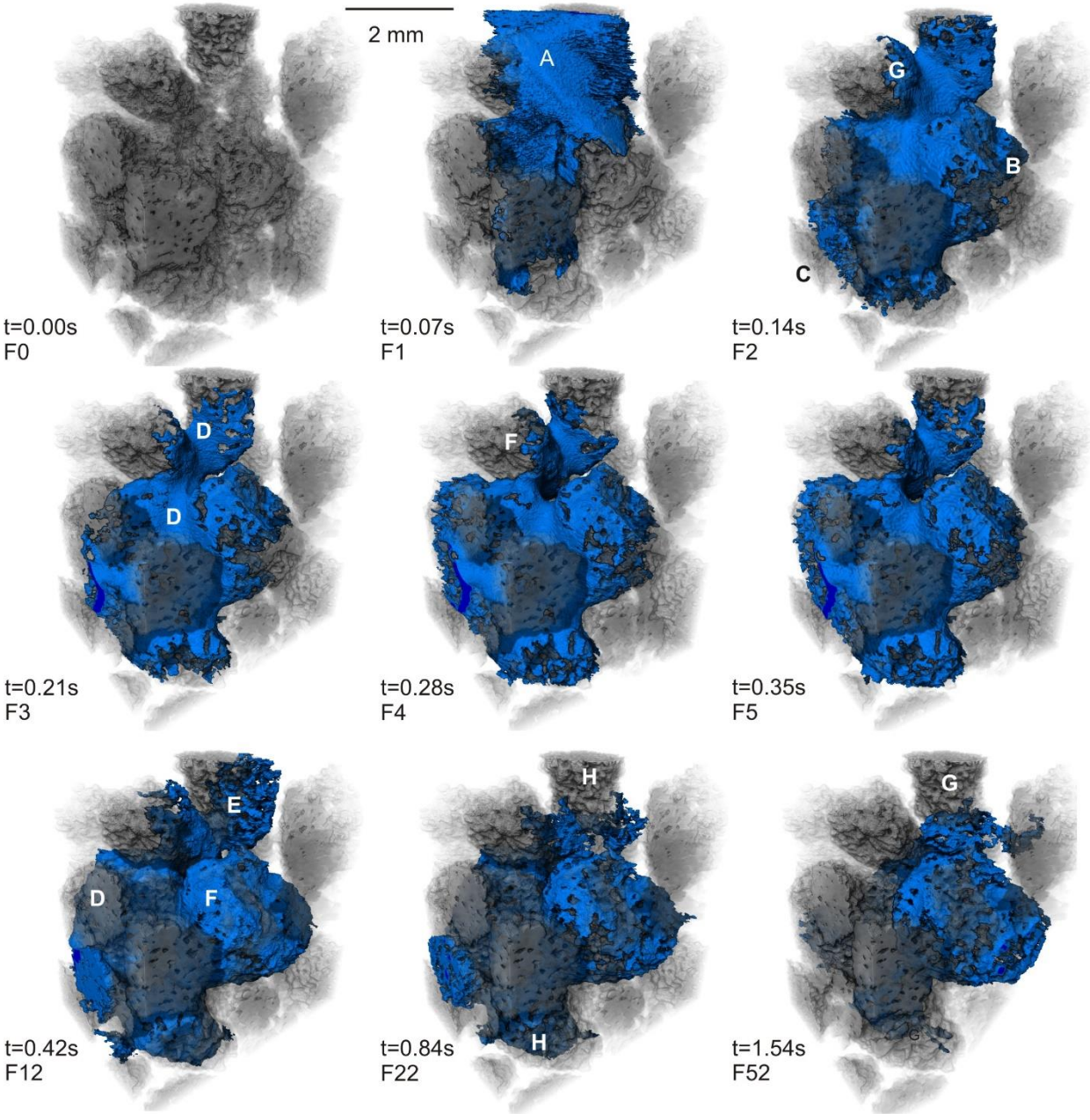

Figure 3: Time series showing the wetting of the sandstone gravel under the first drip. 3D frame acquisition frequency = 0.07/3D volume (14 Hz) The first frame shows the dry sample with the sandstone grains rendered in semi-transparent grey. From the second frae the KI solution is shown in Blue. Note the rapid changes in both the inter- and intra-grain fluid distribution (see text for discussion). The rendered volume is a small sub-volume of the larger data set and shows a volume approximately 3.5 mm x 3.5 mm x 2 mm. Data are from sample LH_9, scan 1

Solid Earth Discuss., doi:10.5194/se-2016-40, 2016
Manuscript under review for journal Solid Earth
Published: 21 March 2016

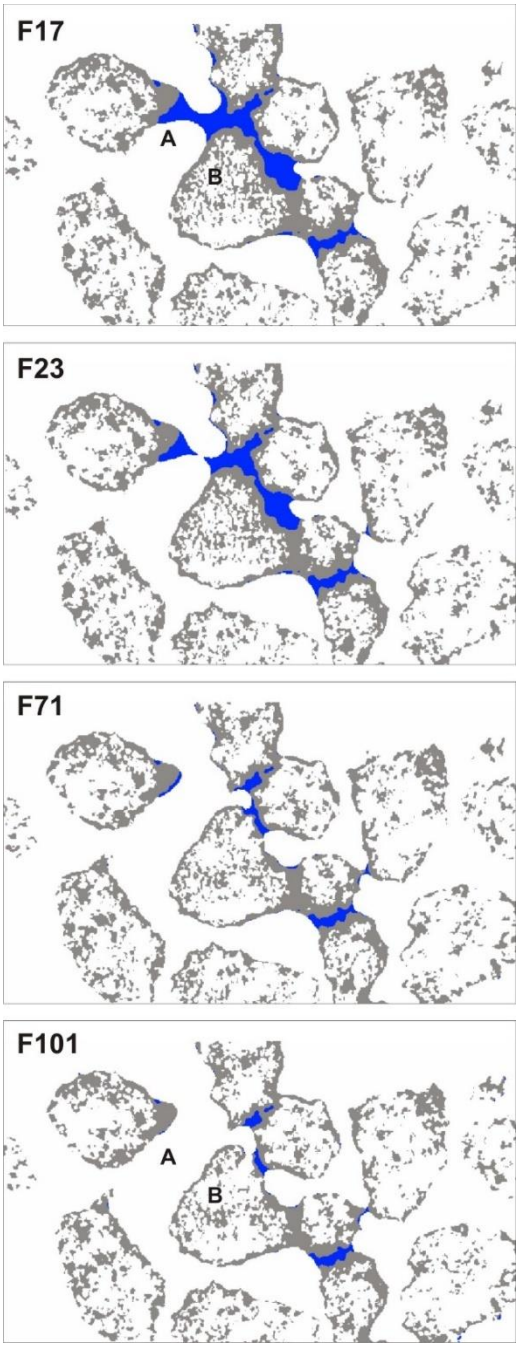

Figure 4: A single vertical 2D slice through the second scan. The frames shown cover the passage of the through the sample. The inter-grain fluid is shown in blue and the intra-grain fluid in grey. Wet rocks = grey, KI solution outside the rocks = blue, air and dry rocks in background. Field of view is 3.5 mm x 2 mm. Data are from sample LH_9, scan 3.

Solid Earth Discuss., doi:10.5194/se-2016-40, 2016
Manuscript under review for journal Solid Earth
Published: 21 March 2016

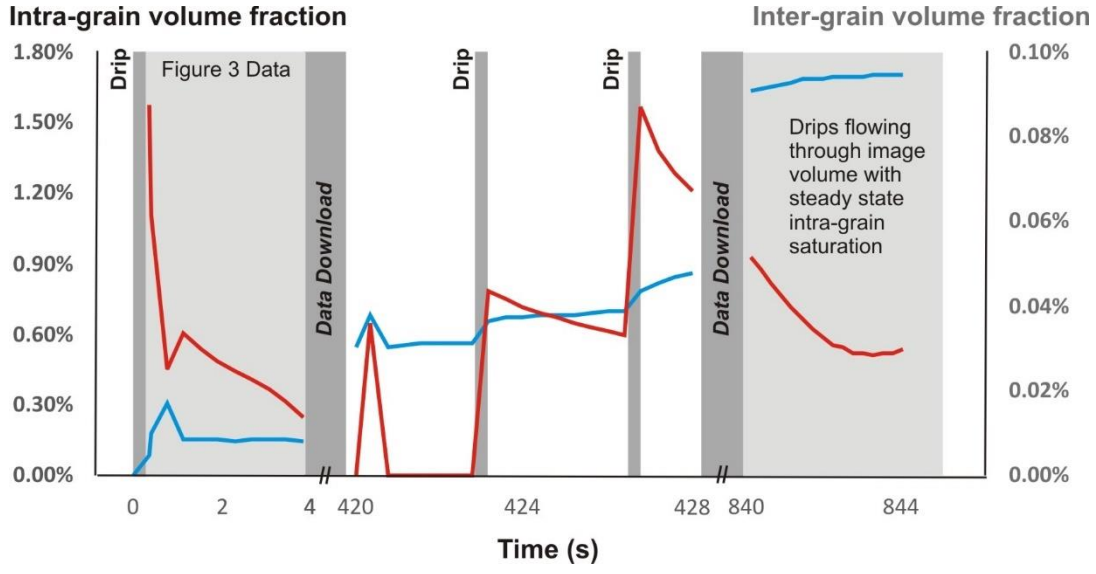

Figure 5: The change in fluid volume within the inter- and intra-grain porosity over the experiment showing the arrival and subsequent equilibration of two drips. After the 1st drip the system equilibrates to very low inter-grain saturation. Data are from sample LH_9, scans 1 to 3.

Solid Earth Discuss., doi:10.5194/se-2016-40, 2016
Manuscript under review for journal Solid Earth
Published: 21 March 2016

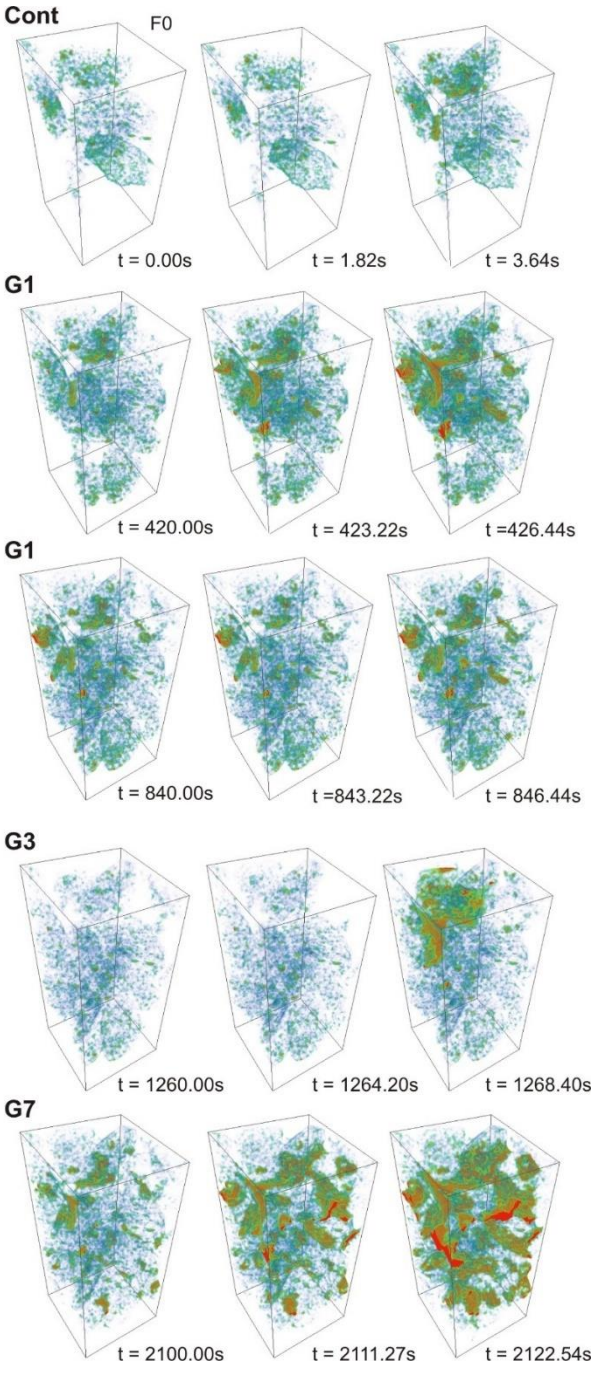

Figure 6:3D renders of a gapped experimental run. For each scan series the first, middle and last frame of each acquisition period is shown. Only the fluid volume has been rendered, with the colour representing the distance to the fluid interface. Cool colours represent small fluid volumes; hot colours represent fluid more than 20 µm from the interface. The field of view is 1.5 mm x 1.5 mm x 3 mm. Data from sample LD_1, scans 1 to 5.

Solid Earth Discuss., doi:10.5194/se-2016-40, 2016
Manuscript under review for journal Solid Earth
Published: 21 March 2016

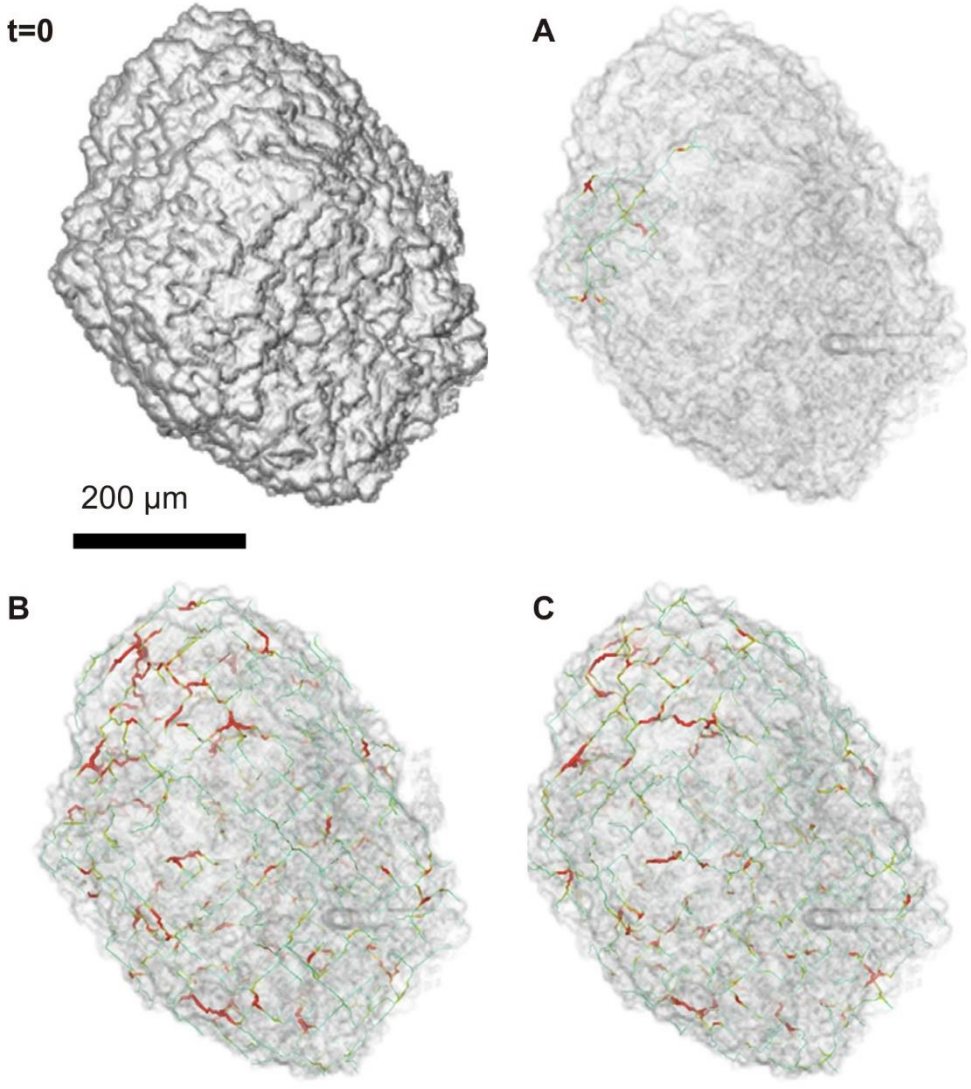

Figure 7: A 3D render of a single grain showing the progression of saturation. The images show the evolution from first contact with the fluid to a steady saturated state over three scans. The colours and the size of tubes representing the pore network correspond to the local volume of the fluid within the pores: thick, red tubes represent the higher local volume; thin, blue tube represents lower local saturation. Data are from sample LD_1, showing the dry scan (t=0) and the final frames of A) scan 1 (continuous), B) scan 2 (G1) and C) scan 3 (G1).

Solid Earth Discuss., doi:10.5194/se-2016-40, 2016
Manuscript under review for journal Solid Earth
Published: 21 March 2016

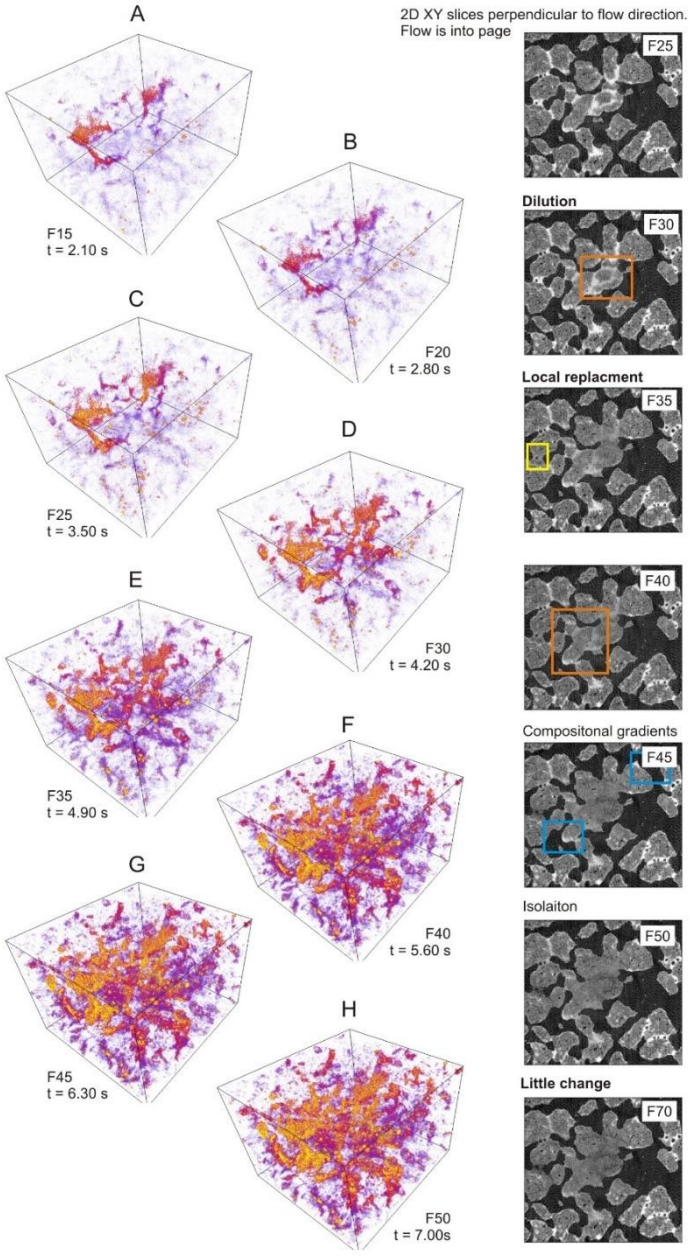

Figure 8: In situ observation of dilution. The 6M saline solution feed is replaced by H_2O at t=0. A-H, 3 D renders of the differential density (greyscale) between the initial saline fluid volume and the saline + water mixture at the times shown. The frame acquisition rate was 0.07s and acquisition frequency was 7 Hz (G1). Data is from sample LD_3, scan 1. Yellow represents complete replacement with H_2O. Cooler colours represent volumes that are undergoing dilution. Volumes remaining at 6M KI are not shown, as they have undergone no change.

Solid Earth Discuss., doi:10.5194/se-2016-40, 2016
Manuscript under review for journal Solid Earth
Published: 21 March 2016

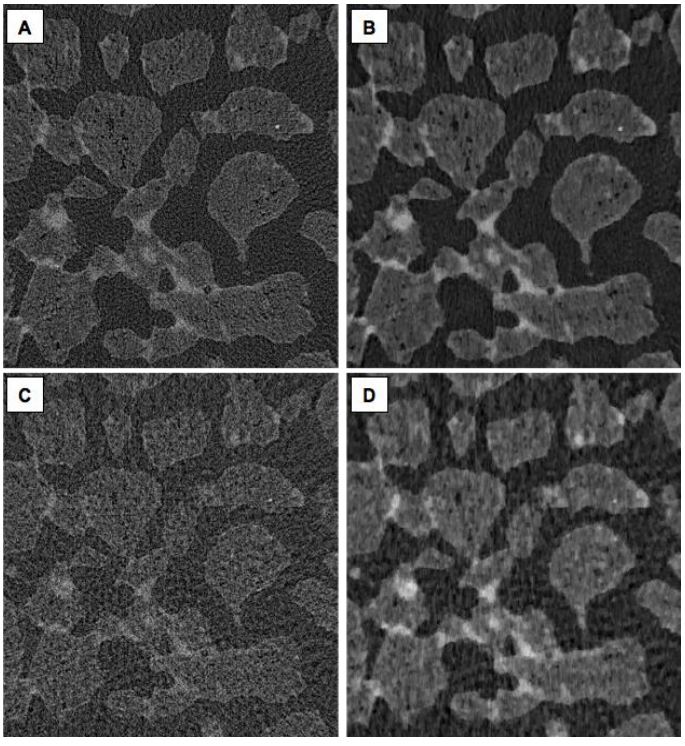

Figure 9: 2D reconstructed slices through a gravel sample using filtered back projection (A, C), and an iterative optimisation method with the total variation regularisation incorporated as prior information (B, D). Reconstructions are obtained using 180 projections (A, B) and 90 projections (C, D). The cropped area shown is approximately 3.5mm x 3.5 mm. Note the increased definition of both the inter- and intra-grain porosity that can be achieved for a given number of projections. Data are from sample LD_3, first frame, scan 1.

Solid Earth Discuss., doi:10.5194/se-2016-40, 2016
Manuscript under review for journal Solid Earth
Published: 21 March 2016

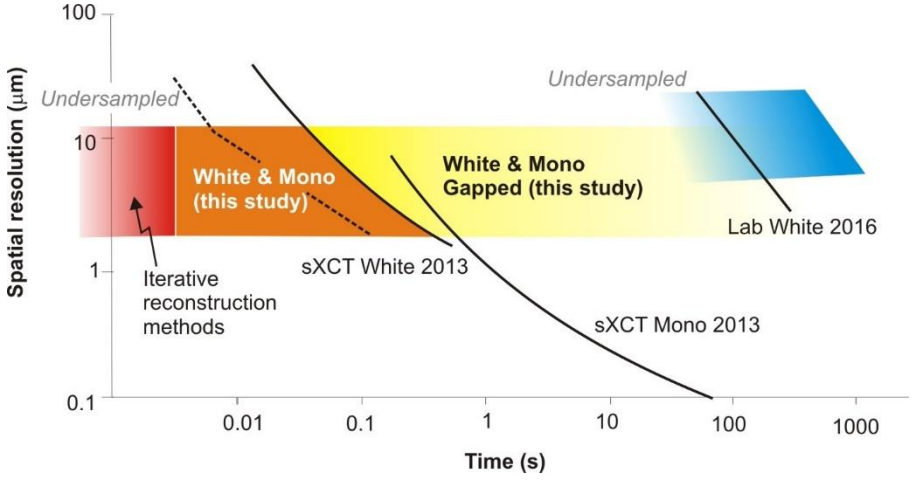

Figure 10: A schematic showing the current state of the art imaging capabilities for synchrotron and laboratory XCT scanning (modified after Bultreys et al.; Maire and Withers, 2014).